Influence of fibre architecture on the tensile, compressive and flexural behaviour of 3D woven composites

S.Dai[a,*], P.R. Cunningham[a], S. Marshall[b], C. Silva[b]

[a] *Department of Aeronautical and Automotive Engineering, School of Aeronautical, Automotive, Chemical and Materials Engineering, Loughborough University, LE11 3TU, UK.*
[b] *M. Wright and Sons Ltd, Quorn Mills, Quorn, Loughborough LE12 8FZ, UK*

Abstract

This paper presents a comprehensive study on the tensile, compressive, and flexural performance of six types of 3D woven carbon-fibre/epoxy composites which were manufactured using a traditional narrow fabric weaving loom and resin transfer moulding. Four orthogonal and two angle-interlock weaves were tested with the primary loading direction parallel to the warp direction. The mechanical performance was found to be affected by the distribution of resin rich regions and the waviness of the load-carrying fibres, which were determined by the fibre architectures. The binding points within the resin rich regions were found to be the damage initiation sites in all weave types under all loading conditions, which were confirmed with both visual observation and digital image correlation strain maps. Among all weave types, the angle interlock weave W-3 exhibited the highest properties under all loading conditions.

Keywords: A. 3-Dimensional reinforcement; B. Mechanical properties; E. Weaving; E. Resin transfer moulding.

1. Introduction

The current trend in composites research in the aerospace and automotive industry is to develop advanced composites using low cost "out-of-autoclave" manufacturing techniques, produce a component with high structural integrity and high delamination resistance, and explore the potential for automated manufacturing processes [1, 2, 3]. Compared to conventional pre-preg layered laminated composites, 3D woven composites provide these advantages. It has been shown by various researchers that the impact resistance, post-impact strength, and delamination toughness are improved by introducing through-thickness binder fibres [1, 4, 5, 6, 7]. However, the in-plane

*Corresponding author. Email: S.Dai@lboro.ac.uk

mechanical properties of 3D woven composites are generally compromised due to the existence of fibre crimping introduced by the weaving process [1, 8]. Three-dimensional woven composites have shown both increases and decreases in elastic modulus, tensile strength, and compressive strength compared with the conventional 2D laminated composites which have comparable in-plane fibre structures (such as similar in-plane fibre volume fraction) [2]. However, due to the limited published data for flexural strength, it is difficult to determine whether the flexural strength is increased or decreased by the through-thickness fibres [2]. Comprehensive experimental studies were carried out on the tensile, compressive, and flexural behaviour of 3D woven composites [7, 9, 10, 11, 12, 13], however more data are required to further understand the behaviour of 3D woven composites with various weave architectures and update with the advances in weaving technology.

The in-plane tensile properties of various types of 3D woven composites have been experimentally characterised and compared with other fibre architectures such as non-crimp fabrics and 2D woven composites [8, 9, 10, 11, 14, 15, 16, 17]. One of the common conclusions drawn by this research is that the tensile properties can be improved by having a minimum waviness in the in-plane fibres, which is affected by the weave architecture. The compressive properties of 3D woven composites were reported to be lower [18], similar [12], and even higher [7] compared to the 2D equivalent composites. It was suggested by Cox et al. [19] that it was more efficient to improve the compressive strength by increasing the geometrical regularity than increasing the fibre volume fraction, which on the other hand results in brittle compressive failure and lower failure strain. The compressive failure was found to initiate around the geometrical flaws and was dominated by fibre kinking which almost always occurred across the entire cross-section of the load-carrying tows [11, 19, 20, 21]. The effect of the weave architectures on the flexural behaviour of 3D woven composites were studied in [9, 12, 22], and the through-thickness binder yarns were found to be effective in resisting delamination crack growth. Kuo [23] conducted flexural tests on two types of 3D orthogonal woven carbon/epoxy composites and concluded that the binder yarn loops at the surface of the fabrics prevent and deflect crack propagation. Adanur and Tam [24] reported that the flexural strength of 3D interlock glass/epoxy composites was higher than 2D laminates.

In this paper, four types of 3D orthogonal woven composites and two types of 3D angle interlock woven composites were manufactured and tested under tension, compression, and three-point bending. The manufacturing process and experimental techniques are described, and the influence of the weaving process on the weave architectures are discussed. The stress-strain and

load-displacement curves under different loading conditions are presented along with the tensile, compressive, and flexural properties, and full-field surface strain distribution maps during tensile tests are illustrated using a digital image correlation system. The results of all six weave architectures are compared and discussed.

2. Materials and manufacture technique

2.1. Manufacturing process

All of the fabric preforms were woven using a traditional narrow fabric weave loom (Muller-NC2-S) by M.Wright & Sons Ltd. Six types of fabrics were produced with the geometric model of the idealised weave architectures generated using TexGen [25] as shown in Figure 1. One design of a 1-by-1 orthogonal weave (W-1), three designs of a 3-by-3 orthogonal weave (W-2.1, W-2.2, and W-2.3), and two types of angle-interlock weaves (W-3 and W-4) were produced. All six weaves used the same type of warp and weft yarns as listed in Table 1, and the binder yarns were different between designs in order to achieve the same amount of fibres in the through-thickness direction. The spacing of the warp tows was kept at 1.535 ends/mm and the weft tow spacing was kept at 1.5 picks/mm for all of the weaves. The nominal thickness was 0.42 mm for the weft tow and 0.40 mm for the warp tow, and the nominal width was 1.7 mm for the warp tow and 2.5 mm for the weft tow. It should be noted that each weft tow consists of two 6k yarns because the loom employed a rapier weft insertion system which feeds one weft yarn during weft insertion and another weft yarn during weft arm retraction.

Each preform was an 80 mm wide, 350 mm long, and 3 mm thick (all dimensions are nominal) strip since it was fabricated using a traditional narrow fabrics weaving loom. Five strips were placed in a rectangular shaped closed mould tool for resin transfer moulding using a Hypaject MK-III RTM system. An 8 mm silicone intensifier was use to fill in the redundant cavity in the mould tool and provide a consolidation pressure. A Gurit Prime 20LV epoxy resin system, which is a two parts epoxy system consisting of resin and slow hardener, was used to infuse the preforms. The resin was degassed and heated up to 30°C in the homogeniser and then injected into the vacuumed and preheated mould tool. The injection pressure was kept at 1 bar before the mould tool was fully filled, and once the resin filled the mould the outlets were locked and the injection pressure was increased to 1.5 bar and kept for 5 min to further fill any possible dry spots. The mould tool was then heated up to 50°C for 16h for curing. The entire manufacturing process including both weaving and moulding were carefully documented and monitored to ensure consistency of the samples.

2.2. Examination of the manufactured weave structures

The manufactured samples were sectioned, polished and examined under an optical microscope. All microscopic samples were randomly selected from the same panel from which the testing samples were cut, and the typical internal and surface fibre geometries of the six weaves are shown in Figure 2 and Figure 3. As can be seen, the actual fibre architectures differ from the idealised designs. For instance, the warp and weft tows were designed to be non-crimp in all of the designs, however the real samples showed a certain degree of waviness, which was quantified for the warp tows as shown in Table 4. Six warp tows were taken for measurement from the microscopic images to give the averaged tow waviness. A more detailed discussion of the weave structures is presented in the following sections.

2.2.1. Binder/warp direction

The actual binder path of the weaves are affected by the interlacing movement which largely depends on the weave architectures. W-1 had the most orthogonally placed binder tows among all four weaves. The 1-by-1 orthogonal weave had a more compact binding structure than the other 3-by-3 weaves since every column of the weft tows were interlaced by the binder yarns in W-1. This compact interlacing sequence resulted in smaller resin rich regions and less free space for the warp tows to move and therefore relatively straight warp tows.

In W-2.1, three weft tows were bound together, which resulted in the merging of these three weft tows forced by the binding movement. Therefore the space designed to be in between two individual weft tows was shifted resulting in the formation of a large resin rich region at each side of the merged tows. Since the binder tows remained tangential to the weft tows at the surface of the weave, the through-thickness portions of the binder tows were then inclined at an angle within the extra space created between the weft tows. This large gap also gave the warp tows more space to expand since there were no weft tows constraining the movement. It is clearly shown in Figure 2 that the warp tow of W-2.1 had a wavy path and expands its cross-section in the through-thickness direction between the two merged weft tows.

Weave W-2.2 and W-2.3 were also 3-by-3 weaves similar to W-2.1 with three weft tows bound together by one binder yarn but in different binding sequences. However, these three weft tows were separated by another binder in the adjacent cell, which kept the weft tow within the vicinity of its designed position. Hence, the weft tow spacing was more evenly distributed in these two weaves, which resulted in smaller resin rich regions and more orthogonally placed binders compared to W-2.1.

Moreover, the warp tows were relatively straight and had a more constant cross-section along the length in these two weaves than in W-2.1. The warp tows in W-2.2 were slightly less crimped than in W-2.3 due to a shorter weft flow as shown in Figure 4. Within the longer weft flow, the weft tows were relaxed and moved towards an adjacent binding point, which then left a gap in between that allowed the warp tow to crimp.

Weave W-3 is an angle-interlock weave with non-interlacing warp tows which had limited crimp. The cross-section of the weft tows in W-3 shifted into a parallelogram-like shape to fit the binder tow path. Since two adjacent binder tows had different paths, the parallel angle of the cross-section also changed in the adjacent cell along the weft direction. Therefore it can be inferred that the weft tow in W-3 had a varying cross-section.

Weave W-4 is an angle-interlock weave with only interlocking binder tows which used the same IMS5131-24k yarns as the warp tows in all other designs. As shown in Figure 2, all binder tows were at an angle and the cross-sections of the weft tows were shaped into various forms by the tensioning force on the 24k binder yarns during the weaving process.

2.2.2. Weft direction

In all of the orthogonal weaves, due to the orthogonal binder insertion, a clear resin channel was left between two weft tows as shown in Figure 3. It can also be seen that W-1 had a evenly spaced resin-rich channel, W-2.1 had the widest resin rich channel, and both W-2.2 and W-2.3 had discontinuous and curved resin channels. The effect of the resin channel on the mechanical performance will be discussed in a later section. In the angle-interlock W-3, the surface resin rich regions were localised around the binding point and did not form a distinctive channel. In W-4, resin rich zones were distributed as "resin pockets" between the weft and binder tows.

The in-plane waviness of the weft tows varies between designs. As shown in Figure 4, the weft tows of W-1, W-2.1, W-3, and W-4 had the least in-plane waviness, because the adjacent binders on these weft tows had the same binding movement which did not force the weft tows to bend in opposite directions. While in W-2.2 and W-2.3, the two adjacent binders had the opposite movement as demonstrated by the arrows in Figure 3. The curvature of the weft tows at the binding points in W-2.2 was larger than in W-2.3, which was caused by the difference in binding sequence between the two weaves.

The samples were also sectioned along the weft direction to reveal the internal weft tow path, as shown in Figure 4. W-1 had the least crimped weft tows among all of the designs due to the compact

binding sequence and the shorter weft flow. As shown in Figure 4, W-2.1 and W-2.2 had shorter weft flows than W-2.3, therefore the out-of-plane waviness of the weft tows in these two weaves was larger than in W-2.3. W-3 also had some extent of out-of-plane waviness in the weft tows, which is caused by the longer weft flow. The weft tows in W-4 had the largest out-of-plane waviness due to the absence of non-interlacing warp tows in this weave architecture. The non-interlacing 24k warp tows in all other designs were changed into angle-interlock tows in W-4. This increased thickness angle-interlock binder yarn also caused the out-of-plane waviness of the weft.

2.3. Measured fibre volume fraction

The nominal thickness of the infused composite panel was 2.78 mm with variations between weave types as listed in Table 2, which were averaged from the 22 mechanical testing samples. The fibre volume fractions of the six types of composites were obtained from matrix burn-off tests. By measuring the weight before and after burn off tests, the overall fibre volume fraction were calculated. The fibre volume fraction of the warp tows and weft tows were measured by separating a dry fabric strip which was long enough to cover at least four complete unit cells, into individual tows and weighing the overall mass of each type of tow. Two dry fabric samples and three composite samples were measured and the averaged results are listed in Table 2. All of the weave architectures except W-3 had a similar overall fibre volume fraction of around 50%, while W-3 had the lowest overall fibre volume fraction and warp fibre volume fraction.

3. Mechanical testing

All samples were cut from the moulded panel using a water jet cutter. Tensile, compression, and flexure tests were conducted on all six weave architectures with the primary loading axis parallel to the warp direction. Five samples were tested for each weave type under each loading condition and the geometries of each type of samples are shown in Table 3.

3.1. Tensile testing

The tensile tests were carried out following ASTM D3039 standard [26] using an Instron 6025 testing machine with a 100 kN load cell as shown in Figure 5. A displacement control of 2 mm/min was applied and one 5 mm long TML-BFLA-5-3 strain gauge was attached in the centre of each specimen along the loading direction to determine the elastic modulus. Since the strain gauge only measures local strain and fails at higher strain, a LaVision 2D digital image correlation (DIC) system was used on two extra samples of each weave in order to obtain full-field strain development

especially in the higher strain regions. Random speckle patterns were applied to these samples using white paint on a matt black base coat, and the DIC camera recorded the deformation at 4 frames/s during loading. All of the samples were loaded until cross-sectional fracture with the load, displacement, and strain data recorded at 2 Hz.

3.2. Compression testing

The compression tests were conducted following the modified ASTM D695 standard [27, 28] using an Instron 6025 with a 100 kN load cell and an anti-buckling guide as shown in Figure 6. In order to achieve an acceptable compressive failure mode a short gauge length of 5 mm was required [27], which was not enough to attach the strain gauges. Therefore two independent tests were conducted to obtain the compressive modulus and strength. The compressive modulus were obtained from strain gauged un-tabbed samples, while the compressive strength were obtained from end-tabbed samples. For each untabbed sample, another sample was cut next to it to obtain the compressive strength. A displacement control of 2 mm/min was applied on each sample and TML-BFLA-2-3 (2 mm) strain gauges were attached in the centre of the un-tabbed specimens.

3.3. Flexure testing

The flexural properties were obtained from three point bending tests. Preliminary tests were carried out on W-1 samples with span-to-thickness ratio of 16, 32, 40, and 60 as suggested by ASTM D790 [29], and five samples were tested with each ratio. It was found that a span-to-thickness ratio of 40:1 provided the least scatter in the flexural modulus and strength results, which was then used to conduct all of the flexural tests. An Instron 8870 with a 25 kN load cell was used to perform the tests as shown in Figure 7, and a 2 mm/min displacement control was applied.

4. Results and discussion

4.1. Tensile testing

Figure 8 shows the stress-strain curves of one example specimen from each weave with the stress and strain recorded until failure, and Table 4 lists the averaged tensile strength and modulus from all seven specimens. As shown in the stress-strain curves, all six samples exhibited linear behaviour at the beginning of loading and non-linear behaviour towards final fracture. For all other five weaves except W-4, the non-linear behaviour was attributed to the damage occurring in the specimens and subsequent load re-distribution, such as matrix cracking. For W-4, the non-linear behaviour was partially caused by the damage and partially caused by the straightening effect of the angled binder

tows. The linear portion of the stress-strain curve (0.1-0.3% strain) was used to calculate the tensile modulus according to ASTM D3039 [26]. Unfortunately the strain gauges on two thirds of the samples failed before the sample reached its tensile strength, possibly because the surface matrix cracks occurred within the gauged regions which resulted in the strain gauges debonding. Therefore failure strain was not obtained through these tests. Although the strain gauges failed, the initial linear portions of the stress-strain curves were still considered to be valid, because these linear regions were at about 0.6% strain (at least 200 data points) away from where the strain gauge started to fail. In addition, it is not uncommon to have strain gauges fail due to surface damage [21, 27, 30]. As can be seen from Table 4, the tensile modulus was affected by the waviness of the warp tows: higher waviness resulted in lower modulus. Since the volume fraction of the load-carrying fibres plays an important role in the mechanical properties of composite materials, the tensile properties were normalised by the warp fibre volume of each weave fibre architecture in order to perform an appropriate comparison. The results were normalised according to Equation 1 and are plotted in Figure 9.

$$P_n = P_{act} \times \frac{28\%}{V_{warp}} \tag{1}$$

where P_n is the normalised material property, P_{act} is the actual material property, V_{warp} is the actual warp fibre volume fraction of each weave, 0.28 is the normalised warp fibre volume fraction averaged from all of the weaves.

Weave W-1 had the second highest normalised tensile strength and the third highest normalised tensile modulus. The compact weave structure of W-1 resulted in less crimped warp tows which led to the higher tensile properties. In addition, this compact pattern also improved the regularity of the weave structure, which resulted in W-1 having the lowest coefficient of variation. A similar weave pattern with different types of yarns was tested in [3] and showed a tensile modulus of 60 GPa and a tensile strength of 953 MPa in the warp direction. The warp yarns used in [3] had lower tensile properties than the warp yarns used in this study, and were also lower in volume fraction.

Weave W-2.1 showed the second lowest tensile modulus and the largest scatter. As discussed earlier, W-2.1 had a large resin rich region between the two merged weft tows and the warp tows had more waviness than other four weaves, which resulted in the lower tensile modulus. The unit cell of W-2.1 was relatively large and the fibre/resin distribution were relatively localised on the surface. Therefore the weave had localised high strain regions within the resin rich zones on the surface of the

samples as shown in Figure 11. The length of the strain gauge (5 mm) was not long enough to cover both the resin and fibre regions (10 mm) in this particular weave. Therefore the resultant modulus was artificially lower from the samples with the strain gauge that only covered the resin rich region, and artificially high modulus was obtained from the samples with the strain gauge covering the fibre region. This resulted in the larger coefficient of variation of W-2.1 and also explained the fact that the tensile modulus data had higher scatter than the tensile strength data. The large resin rich channels and crimped warp tows in W-2.1 were reduced by varying the binding sequence, as can be seen in W-2.2 and W-2.3, which resulted in higher tensile modulus of these two weaves. In addition, W-2.2 had a higher tensile modulus than W-2.3 due to its less crimped warp tow. However the tensile strength of W-2.2 was lower than W-2.3 and even W-2.1, which was inferred to be caused by the larger extent of fibre damage during the weaving process due to its less regular weave pattern than W-2.1 and W-2.3, although this has not been confirmed.

Based on the normalised results, W-3 was the highest in both tensile modulus and tensile strength. The compact weft tow placement and the angled binders resulted in less crimped warp tows which led to a higher tensile modulus. The weave architecture also had less and smaller resin rich regions which were found to be the damage initiation sites in the other weaves. Therefore the fewer damage initiation sites resulted in higher tensile strength of W-3.

Weave W-4 exhibited a large extent of non-linearity after about 0.5% strain due to the absence of straight load-carrying warp fibres. The angle-interlock binders started to straighten up during loading, which caused the non-linear behaviour and matrix failure in the resin pockets and then induced failure. Therefore W-4 had the lowest tensile properties among all of the weaves.

Figure 11 shows the strain distribution maps obtained at the averaged strain level of approximately 0.5% strain and at the last frame before fracture, along with the corresponding weave pattern on the left. A 50 mm long virtual strain gauge was attached on the strain map to give the averaged strain within the gauge area. As shown in the strain maps, the strain distribution was largely affected by the weave patterns. Localised high strain regions were detected near the binding points within the resin rich zones where matrix cracks were first visually observed. Two of the samples failed within the DIC monitored region and the final fracture sites are illustrated on the strain maps in these two samples (W-2.1 and W-2.2) in Figure 11. In W-1 and W-2.1, high strain regions were detected within the resin rich channels at an average strain of around 0.5%. W-3 showed a relatively uniform strain distribution with a few strain concentration regions around the binding

points. In all other weaves, the high strain regions concentrated near the binding points since there were no clear connected resin rich channels. As can be seen from Figure 11 (a) and (e), the left side of the specimens showed higher strain than the right side at lower strain level, and this difference almost vanished at higher strain levels. This was possibly caused by the misalignment between the specimen and the DIC camera. The strain caused by this misalignment was lower than the strain at higher stress level, hence became less noticeable. Since the purpose of the DIC was only to qualitatively characterise the strain distribution, this strain difference was neglected. However, more care should be taken in positioning the camera and the specimens in future DIC tests.

The binder tow straightening and matrix cracking around the binding points were visually observed on the surface of the specimens in all weave types. According to the strain distribution maps, strain concentration zones located around the binding points where the binder fibres changed directions, and therefore the matrix cracks initiated within these strain concentration regions. In all of the orthogonal weaves, the matrix cracks initiated around the binding points, propagated along the resin rich channel, and then coalesced together into a longer transverse crack across the width of the sample. In W-1 and W-2.1, warp tow debonding was visually observed through the resin channels after matrix cracking. It was also observed in W-2.1 that the matrix crack initiated inside the weft tow and propagated to the boundary of the weft tow and formed a delamination crack between the weft tow and the warp/binder tow. The stress levels at which these cracks were observed were recorded in some of the samples. The cracks appeared at the edges in W-2.1 at 489 MPa, in W-2.2 at 787 MPa, and in W-4 at 422 MPa, and surface indentation caused by the binder tow straightening was found in W-3 at 422 MPa. However, since these cracks were only detected visually, the initiation stress of these cracks were inconclusive and cannot be used for comparison.

The final tensile failure was the breakage of the warp tows, which occurred along the coalesced matrix cracks within the resin channels. Since the resin channel was curved in W-2.2 and W-2.3 as shown in Figure 3, the final fracture surface followed the curved weft tows in these two weaves. Figure 10 shows the cross-sections parallel to the loading direction in the vicinity of final fracture sites. It can be seen that matrix cracks within the weft tows occurred in all weave types. Clear separation between warp and weft layers was observed in W-1, W-2.1, and W-2.2.

The weaves with more compact architectures (W-1 and W-3) exhibited higher tensile properties, because the compact structures provide less crimped fibre (W-1) and fewer damage initiation sites (W-3). The weave without non-interlacing fibres (W-4) showed the lowest tensile properties since the

benefit of the reinforcement lies in the fibre direction, which was not fully utilised in W-4.

4.2. Compression testing

Figure 12 shows the typical compressive load and displacement curves of the end-tabbed samples of the six weave architectures. Similar to the tensile properties, W-4 exhibited lower compressive properties than other weaves due to the absence of non-crimp fibres in the loading direction. However, it can be seen from the load-displacement curves that the W-4 sample can still carry load at about 75% of its maximum strength while all other weaves had failed completely. It was also observed during testing that the failure process of W-4 was less catastrophic than the other weaves. The averaged compressive properties for all weaves are listed in Table 5 and the normalised results are shown in Figure 13. As can be seen that W-3 and W-4 were the highest and lowest in compressive modulus and strength, all four orthogonal weaves had similar compressive strength, and W-2.1 had the lowest compressive properties among the orthogonal weaves. Since the compression tests were sensitive to misalignment and the length of the strain gauge (2 mm) was shorter than the length of the unit cell (up to 10 mm), the scatter of the compressive properties data was relatively high. Figure 14 shows the fracture sections of the samples from the compressive strength tests. The main compressive failure features included matrix cracking, delamination, warp tow fracture which was the final fracture feature for all weaves except W-4.

In W-1 the delamination crack occurred in between every two layers and propagated for at least two unit cells before being impeded by the binder tows. In W-1 the binder tows were placed between every other weft tow therefore the delamination crack had to break all of the binder tows to propagate to the adjacent cells, which results in a shorter delamination crack than W-2.1.

Weave W-2.1 had longer delamination cracks since the through-thickness binder interlaced three weft tows together with no other binder inserted in between to prevent the crack growth. The delamination crack length was reduced in W-2.2 and W-2.3, which was attributed to the different binding sequence with more frequent binder insertion. Although in W-2.2 and W-2.3 the binder tow also interlaced three weft tows together similar to W-2.1, another binder tow was inserted within these three weft tows in the adjacent cell, which resisted the crack propagation in the adjacent cell and eventually reduced the crack length.

Weave W-3 also had longer delamination cracks, because the binder tows in W-3 were at an angle to the crack, which did not prevent crack propagation as effectively as the orthogonal binders. In addition, the delamination crack was deflected by the binder tow and propagated from between the

first warp layer and the second weft layer to between the second weft layer and the middle warp layer, as shown by the arrows in Figure 14.

It was visually observed in W-4 that cracks initiated at the boundary of the binder tows first, which caused separation between the interlaced tows and resulted in the loss of load-bearing capacity. Since there were no distinctive layers and all binders and weft tows were interlaced, W-4 did not have any delamination cracks. The crack shown in Figure 14 is not considered as a delamination crack since its width did not extend along the width of the sample due to the interlacing binder in the adjacent cell.

The weave with the least crimped tows (W-3) showed higher compressive properties, however it exhibited longer delamination cracks due to the angled binder tows. The four orthogonal weaves showed similar compressive strength with various extent of delamination which can be reduced by changing the binding sequence. W-4 offered the lowest compressive properties due to the absence of non-crimp warp tows but exhibited non-catastrophic failure.

4.3. Flexure testing

The typical stress-strain curves for the six weaves under three-point bending load are plotted in Figure 15, and the actual and normalised flexural properties are presented in Table 6 and Figure 16. Since the span-to-thickness ratio was higher than sixteen and the displacement was larger than 10% of the span, the flexural stress was calculated based on Equation 2 to correct the influence of excessive end-forces induced by large span-to-thickness ratio according to ASTM D790 [29]. The flexural strain was also calculated using Equation 3.

$$\sigma_f = (3PL/2wt^2)\left[1 + 6(D/L)^2 - 4(D/L)(t/L)\right] \tag{2}$$

$$\varepsilon_f = 6Dt/L^2 \tag{3}$$

where σ_f is the flexural stress, P is the applied load, L is the support span, w and t are the width and thickness of the sample, D is the displacement, and ε_f is the strain at the centre of the specimen.

In all of the weaves, the flexural modulus was lower than the tensile and compressive modulus, and the flexural strength was higher than the compressive strength even though the final flexural fracture was caused by compressive failure. Similar testing results were reported by Wang and Zhao [12] on a similar orthogonal 3D woven composite. One possible explanation for the lower flexural modulus is that the middle warp tow passed through the bending neutral plane and therefore was not fully loaded as it did under tensile loading. Therefore one of the three main load-carrying tows

was not fully utilised under flexural loading, which resulted in the lower flexural modulus. The higher flexural strength might also be caused by the uneven distribution of reinforcement in the through-thickness direction. The reported flexural strength was the stress on the outer surface, which was calculated using the classical beam theory for isotropic material. Due to the inhomogeneity in the through-thickness direction, this calculated stress was not the stress in the warp tows which failed in compression. In addition, the reported compressive strength was also an averaged stress over the entire cross-section not the stress within the failed warp tows. Since there were no well-established methods to estimate the stress within a tow in a 3D woven composite, the flexural strength can not be compared directly with compressive or tensile strength.

As can be seen from Figure 15, all weave types exhibited a linear stress-strain behaviour at the beginning of loading, and showed some non-linear behaviour after about 0.01 strain. All of the weaves except W-4 exhibited a load drop once they reached flexure strength, which was caused by the brittle fracture of the load-carrying warp tows on the compression side of the specimen. Since W-4 did not have any straight warp fibres, therefore no catastrophic load-carrying fibre breakage occurred. However the flexural properties of W-4 were the lowest among all weaves. W-2.1 and W-3 had higher flexural properties as listed in Table 6, and were still the higher weaves in the normalised results as shown in Figure 16 due to the angled binder. The flexural properties of W-2.1 were higher than the other orthogonal weaves while its tensile properties were relatively low. A possible explanation is that the angle of the binder tow played a more important role in bending than the warp tow waviness. The binder tow in W-2.1 was at an angle similar to W-3 rather than being orthogonal as shown in Figure 2. Under flexural loading, the binder tow did not straighten and induce cracks as in the tensile tests, instead it acted as a "truss" and improved the bending properties. Therefore the weaves with angled binder tows (W-3 and W-2.1) showed higher flexural modulus.

Figure 17 shows the failed sections of all six weave types. The failure consisted of the matrix cracking near the binding points, delamination, and warp tow fracture which occurred on the compression side under the loading point. Delamination occurred in between the first warp layer and the second weft layer in all of weaves except W-4 and the length of the delamination cracks varied between designs. W-2.1 and W-3 had the longest delamination cracks among all and relatively shorter delamination was found in W-2.2 and W-2.3.

Weave W-1 exhibited a longer delamination crack than W-2.2 and W-2.3. W-1 was designed to have the same amount of fibres in the through-thickness direction within a same area as the other

orthogonal weaves. Therefore the delamination crack should break the same amount of through-thickness fibres within the same region for all orthogonal weaves. In addition, the through-thickness binder tows occurred in between every two weft tows in W-1, which was more frequent than in other orthogonal weaves. However, W-1 used 1k yarns as binders while all other orthogonal weaves used 3k yarns which required more energy to break. It is shown in Figure 17 that the binder tows in W-1 were fractured by the delamination crack while in W-2.2 and W-2.3 the binder tows deflected the crack and were not fractured by delamination. In addition, the through-thickness fibres were placed closely and evenly along the weft direction. Therefore the delamination crack would have an even propagation front, which promoted a steady crack growth and hence a longer crack.

For W-2.1, although it had the same number of binder tows as W-2.2 and W-2.3, it did not have a wide distribution of the through-thickness binder fibres. The through-thickness portions of the binder tows in W-2.1 were all placed within the same binding lines along the same weft tows. Therefore in between two adjacent binding points along the binder, there were no through-thickness fibres resisting delamination, which resulted in a longer delamination. While in W-2.2 and W-2.3, the delamination crack was arrested or retarded by the binder tows in the adjacent cells.

In W-3, the binder tows were at an angle, so they did not prevent crack propagation as effectively as the orthogonal binders due to their shorter and angled through-thickness portions. Also the spacing between two binding points in the warp direction was longer in this angle-interlock weave than in the orthogonal weaves. This larger spacing also caused a longer delamination crack since the delamination can propagate further before getting impeded by the binder tows at the next binding point.

Weave W-4 had the lowest flexural properties among all weave types due to the absence of non-interlacing warp tows. However, W-4 exhibited a more gradual failure process while all other weaves failed catastrophically.

The weave with angled binder tows (W-3 and W-2.1) showed higher flexural properties, however they experienced longer delamination cracks. The angled binder was inferred to increase the flexural properties by acting as a truss, however further tests are required to confirm this. The weave without non-interlacing fibres (W-4) showed the lowest flexural properties but failed progressively.

5. Conclusions

The main objective of this study was to understand the effect of weave architecture and binder placement on the behaviour of the 3D woven composites. Six types of 3D woven carbon fibre composites with the same types of fibres were manufactured using a traditional narrow fabrics weaving loom and resin transfer moulding technique. The tensile, compressive, and flexural modulus and strength in the warp direction of all six weave architectures were experimentally characterised in this work, and the influence of weave architectures on the behaviour of 3D woven composites was revealed. Based on the experimental observations and analysis the following conclusions are made:

1. The waviness of the tows were determined by the weave architectures during the weaving process even though all warp and weft tows were ideally designed to be non-crimp. A compact binding sequence resulted in less crimp in the warp tows such as in W-1 and W-2.2. Longer weft flows with the two adjacent binder tows having opposite binding movement caused the in-plane waviness of the weft tows.
2. The tensile properties of the 3D woven composites were affected by the waviness of the load-bearing fibres. One-by-one orthogonal W-1 and angle-interlock W-3 had higher tensile modulus (78.26 GPa and 79.81 GPa) and tensile strength (1370.92 MPa and 1276.24 MPa) due to their less crimped warp tows. The angle-interlock W-4 showed non-linear stress-strain behaviour due to the absence of non-interlacing warp fibres and the straightening effect of the binders. Two-dimensional strain maps obtained from a DIC system showed strain concentration zones around the binding points where matrix cracks were visually observed.
3. Weave W-3 had the highest compressive properties but also longer delamination crack. All of the orthogonal weaves had similar compressive strength, however W-2.1 had lower compressive modulus due to its crimped warp tows. Delamination occurred to all samples with straight warp tows, and was longer in W-3 and W-2.1 which had longer distance between two binding points. The delamination length can be reduced by changing the binding sequence to one with shorter binder spacing.
4. The flexural properties were found to be higher in W-2.1 and W-3, which was inferred to be caused by the angled binder acting as a truss. However the delamination cracks were longer in these two weaves due to binding arrangement. More tests are required to further understand the flexural strengthening mechanism.

5. Overall, the angle-interlock W-3 exhibited the best performance under all three loading conditions however it had the longest delamination crack among all weaves under both compression and bending loading.

Acknowledgements

This research project is supported by the Aeronautical and Automotive Engineering Department of Loughborough University and M. Wright & Sons Ltd. The help and support of the department staff and M. Wright & Sons Ltd are gratefully acknowledged.

References

[1] L. Tong, A. P. Mouritz, M. K. Bannister, 3D Fibre Reinforced Polymer Composites, 3D Fibre Reinforced Polymer Composites, Elsevier Science, Oxford, 2002, Ch. 5, pp. 107–136.

[2] A. P. Mouritz, B. N. Cox, A mechanistic interpretation of the comparative in-plane mechanical properties of 3D woven, stitched and pinned composites, Composites Part A: Applied Science and Manufacturing 41 (6) (2010) 709–728.

[3] A. E. Bogdanovich, M. Karahan, S. V. Lomov, I. Verpoest, Quasi-static tensile behavior and damage of carbon/epoxy composite reinforced with 3D non-crimp orthogonal woven fabric, Mechanics of Materials 62 (2013) 14–31.

[4] J. N. Baucom, M. A. Zikry, Low-velocity impact damage progression in woven e-glass composite systems, Composites Part A: Applied Science and Manufacturing 36 (5) (2005) 658–664.

[5] F. Chen, J. M. Hodgkinson, Impact behaviour of composites with different fibre architecture, Proceedings of the Institution of Mechanical Engineers, Part G: Journal of Aerospace Engineering 223 (7) (2009) 1009–1017.

[6] G. A. Bibo, P. J. Hogg, The role of reinforcement architecture on impact damage mechanisms and post-impact compression behaviour, Journal of Materials Science 31 (5) (1996) 1115–1137.

[7] J. Brandt, K. Drechsler, F. J. Arendts, Mechanical performance of composites based on various three-dimensional woven-fibre preforms, Composites Science and Technology 56 (3) (1996) 381–386.

[8] D. S. Ivanov, S. V. Lomov, A. E. Bogdanovich, M. Karahan, I. Verpoest, A comparative study of tensile properties of non-crimp 3D orthogonal weave and multi-layer plain weave e-glass composites. part 2: Comprehensive experimental results, Composites Part A: Applied Science and Manufacturing 40 (8) (2009) 1144–1157.

[9] S. Chou, H.-C. Chen, H.-E. Chen, Effect of weave structure on mechanical fracture behavior of three-dimensional carbon fiber fabric reinforced epoxy resin composites, Composites Science and Technology 45 (1) (1992) 23–35.

[10] F. Stig, S. Hallstrom, Assessment of the mechanical properties of a new 3D woven fibre composite material, Composites Science and Technology 69 (11-12) (2009) 1686–1692.

[11] B. N. Cox, M. S. Dadkhah, W. L. Morris, J. G. Flintoff, Failure mechanisms of 3D woven composites in tension, compression, and bending, Acta Metallurgica et Materialia 42 (12) (1994) 3967–3984.

[12] Y. Wang, D. Zhao, Effect of fabric structures on the mechanical properties of 3D textile composites, Journal of Industrial Textiles 35 (2006) 239–256.

[13] S. Dai, P. R. Cunningham, S. Marshall, C. Silva, Mechanical behaviour of 3D woven composites under tension, compression and bending, in: Proceedings of ICCM-19, CACSMA, Montreal, Canada, 2013, pp. 2812–2820.

[14] B. N. Cox, M. S. Dadkhah, W. L. Morris, On the tensile failure of 3D woven composites, Composites Part A: Applied Science and Manufacturing 27 (6) (1996) 447–458.

[15] H. Gu, Z. Zhili, Tensile behavior of 3D woven composites by using different fabric structures, Materials & Design 23 (7) (2002) 671–674.

[16] S. V. Lomov, A. E. Bogdanovich, D. S. Ivanov, D. Mungalov, M. Karahan, I. Verpoest, A comparative study of tensile properties of non-crimp 3D orthogonal weave and multi-layer plain weave e-glass composites. part 1: Materials, methods and principal results, Composites Part A: Applied Science and Manufacturing 40 (8) (2009) 1134–1143.

[17] P. J. Callus, A. P. Mouritz, M. K. Bannister, K. H. Leong, Tensile properties and failure mechanisms of 3D woven grp composites, Composites Part A: Applied Science and Manufacturing 30 (11) (1999) 1277–1287.

[18] T. R. Guess, E. D. R. Jr., Comparison of interlocked fabric and laminated fabric kevlar 49/epoxy composites, Journal of Composites Technology and Research 7 (4) (1985) 136–142.

[19] B. N. Cox, M. S. Dadkhah, R. V. Inman, W. L. Morris, J. Zupon, Mechanisms of compressive failure in 3D composites, Acta Metallurgica et Materialia 40 (12) (1992) 3285–3298.

[20] W. S. Kuo, T. H. Ko, Compressive damage in 3-axis orthogonal fabric composites, Composites Part A: Applied Science and Manufacturing 31 (10) (2000) 1091–1105.

[21] W. S. Kuo, T. H. Ko, C. P. Chen, Effect of weaving processes on compressive behavior of 3D woven composites, Composites Part A: Applied Science and Manufacturing 38 (2) (2007) 555–565.

[22] L. Jin, Z. Niu, B. C. Jin, B. Sun, B. Gu, Comparisons of static bending and fatigue damage between 3D angle-interlock and 3D orthogonal woven composites, Journal of Reinforced Plastics and Composites 31 (14) (2012) 935–945.

[23] W. S. Kuo, The role of loops in 3D fabric composites, Composites Science and Technology 60 (9) (2000) 1835–1849.

[24] S. Adanur, C. A. Tam, On-machine interlocking of 3D laminate structures for composites, Composites Part B: Engineering 28 (5-6) (1997) 497–506.

[25] University of Nottingham, TexGen, on-line (August 2013).

[26] ASTM International, ASTM D3039/3039M standard test method for tensile properties of polymer matrix composite materials (2008).

[27] D. O. Adams, A comparison of CEN and ASTM test methods for composite materials (June 2004).

[28] ASTM International, ASTM D695 standard test method for compressive properties of rigid plastics (2010).

[29] ASTM International, ASTM D790 standard test methods for flexural properties of unreinforced and reinforced plastics and electrical insulating materials (2010).

[30] G. Zhou, G. A. O. Davies, Characterization of thick glass woven roving/polyester laminates: 1. tension, compression and shear, Composites 26 (8) (1995) 579–586.

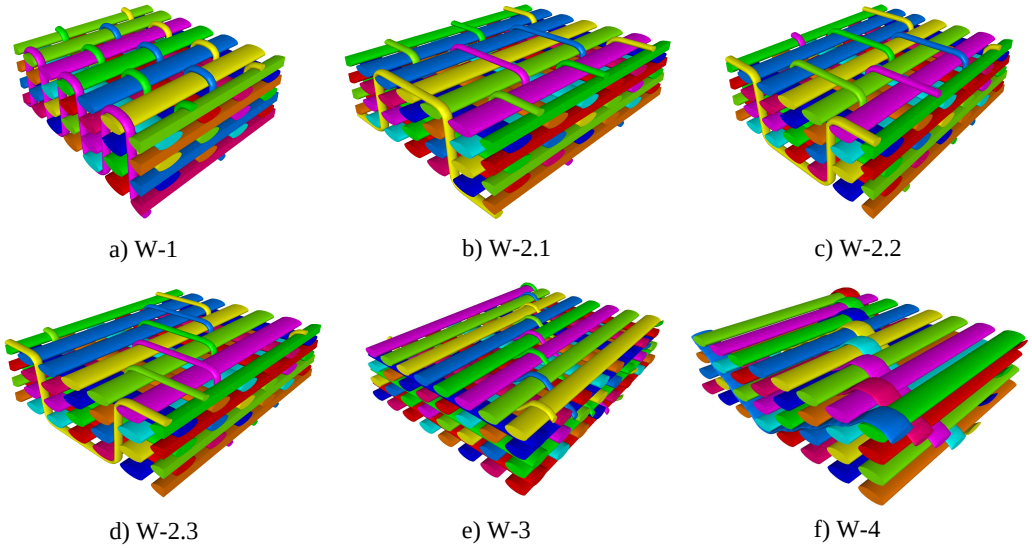

Figure 1: Idealised weave architectures generated using TexGen.

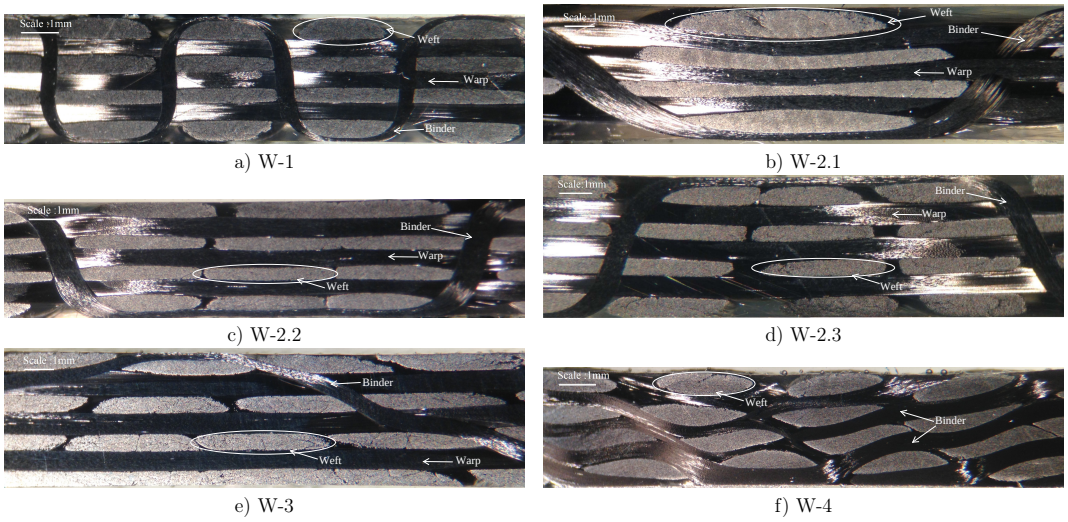

Figure 2: Internal geometry of woven composites, section parallel to binder direction.

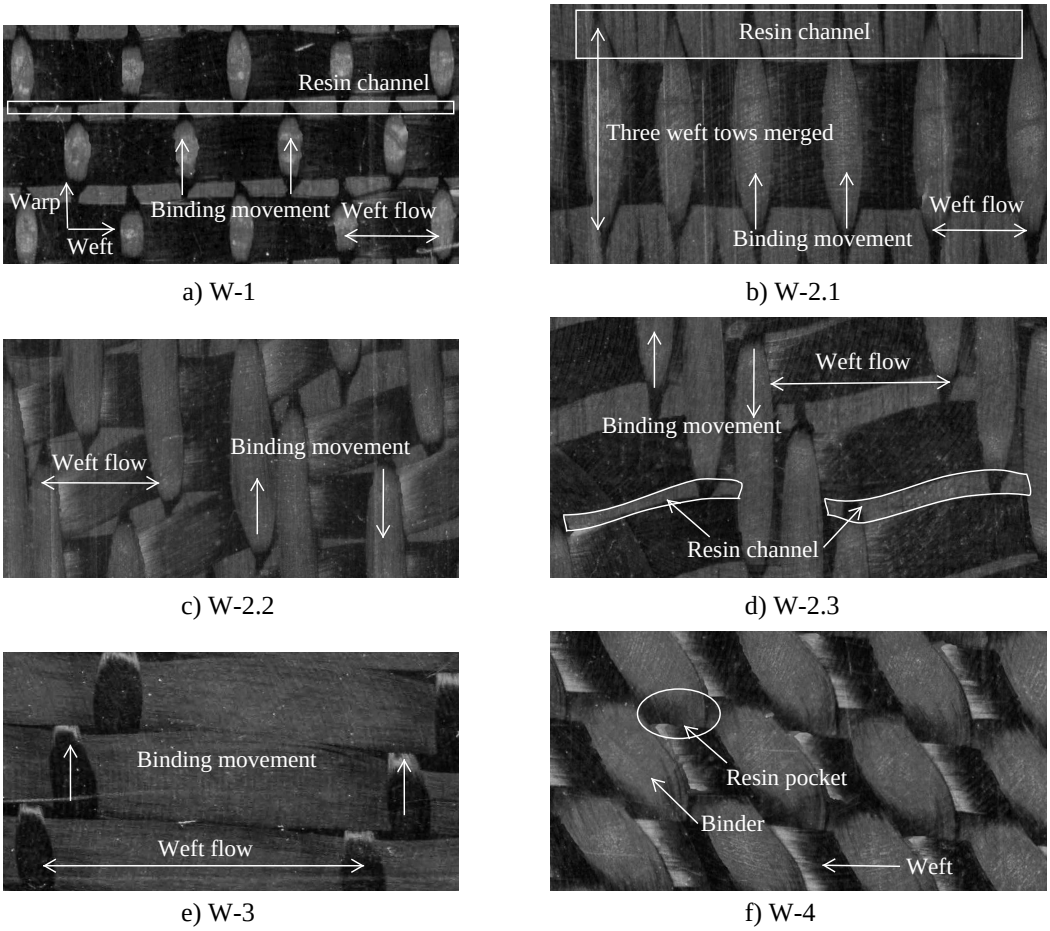

Figure 3: Surface geometry of woven composites.

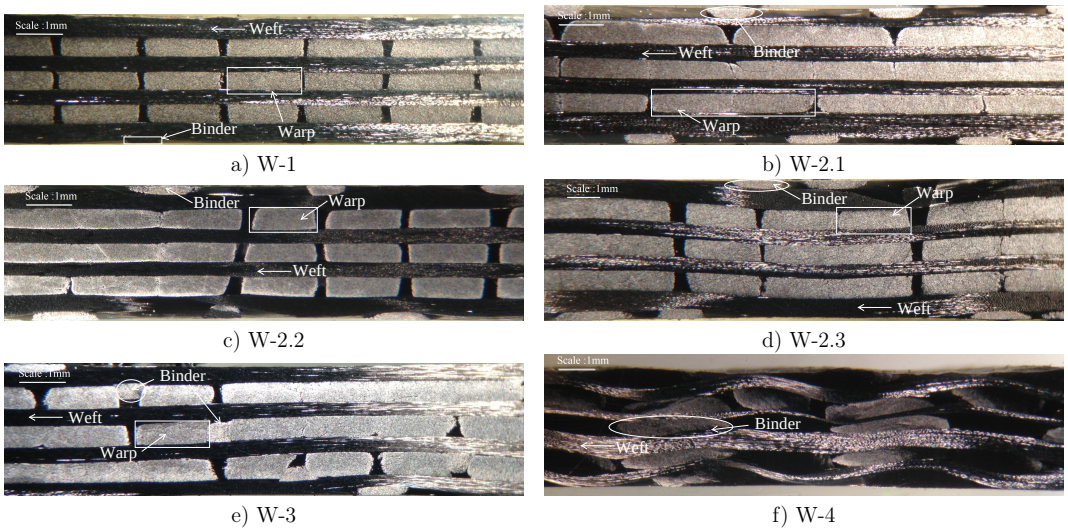

Figure 4: Internal geometry of woven composites, section parallel to weft direction.

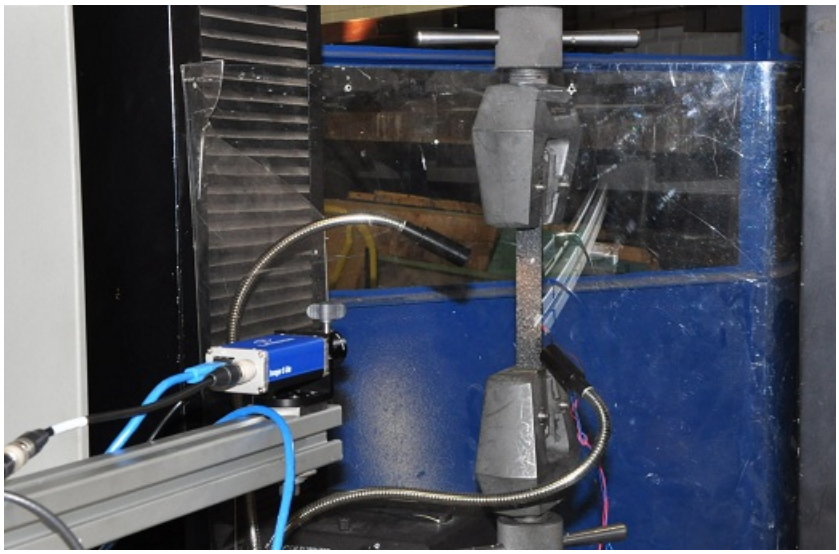

Figure 5: Experimental set-up for tensile tests with a DIC system.

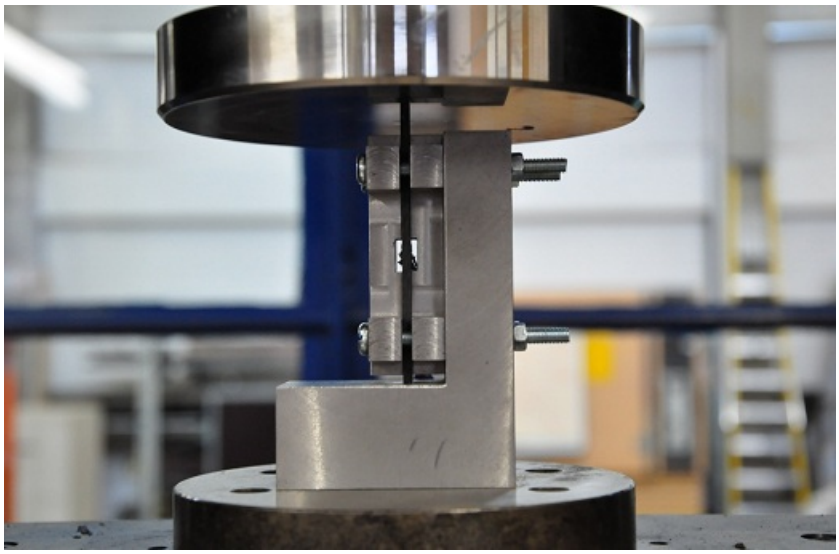

Figure 6: Experimental set-up for compression modulus tests.

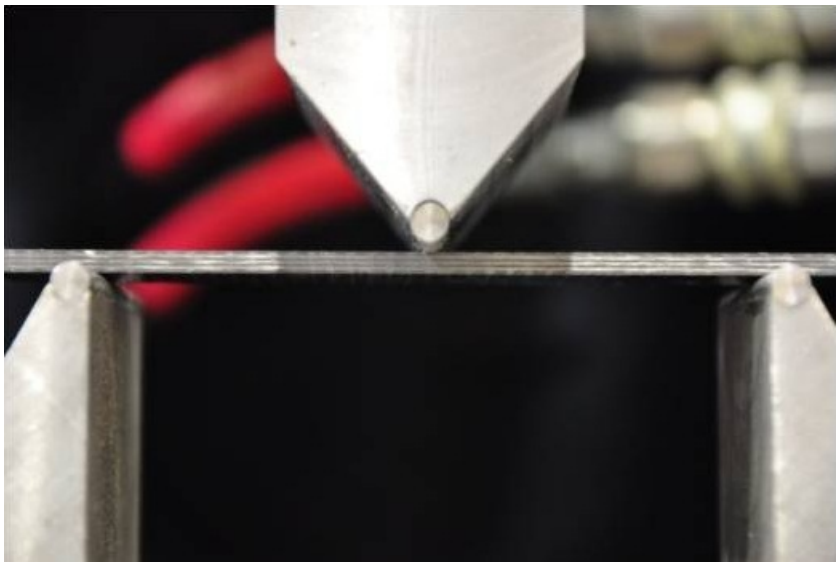

Figure 7: Experimental set-up for flexure tests.

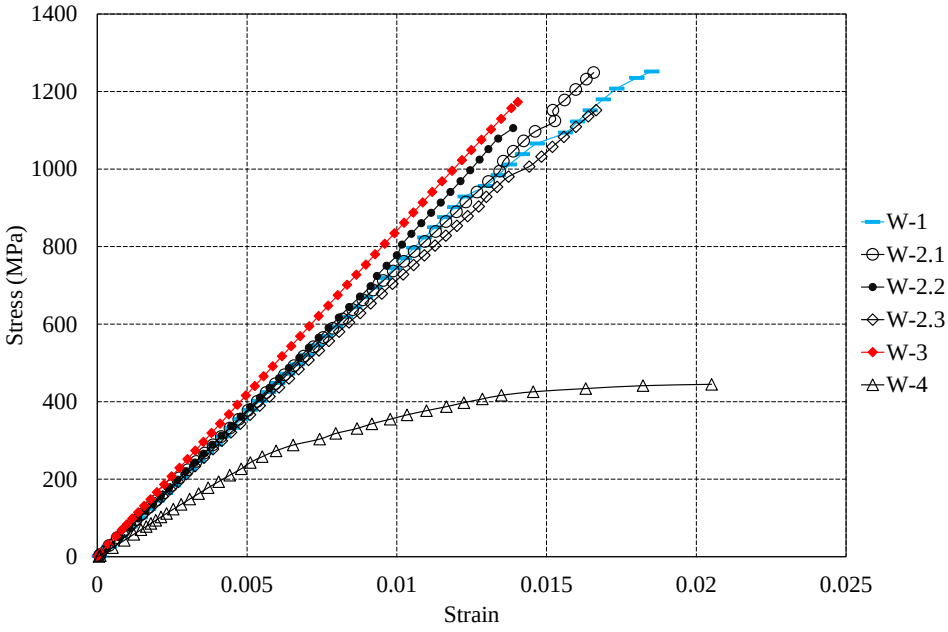

Figure 8: Typical stress-strain curves for all six types of woven composites under tension.

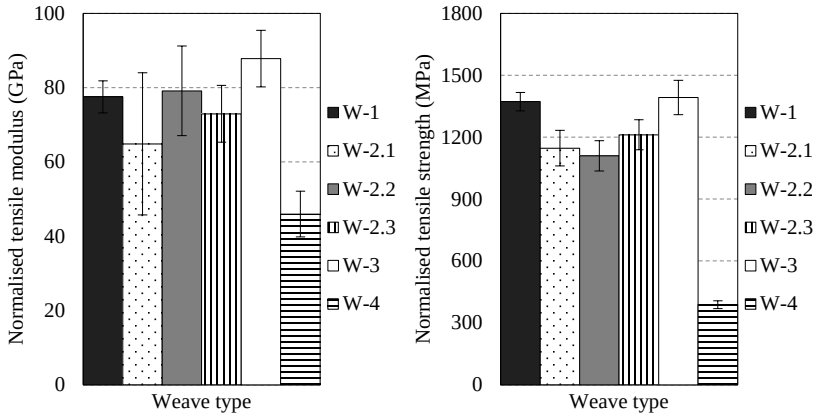

Figure 9: Normalised tensile properties.

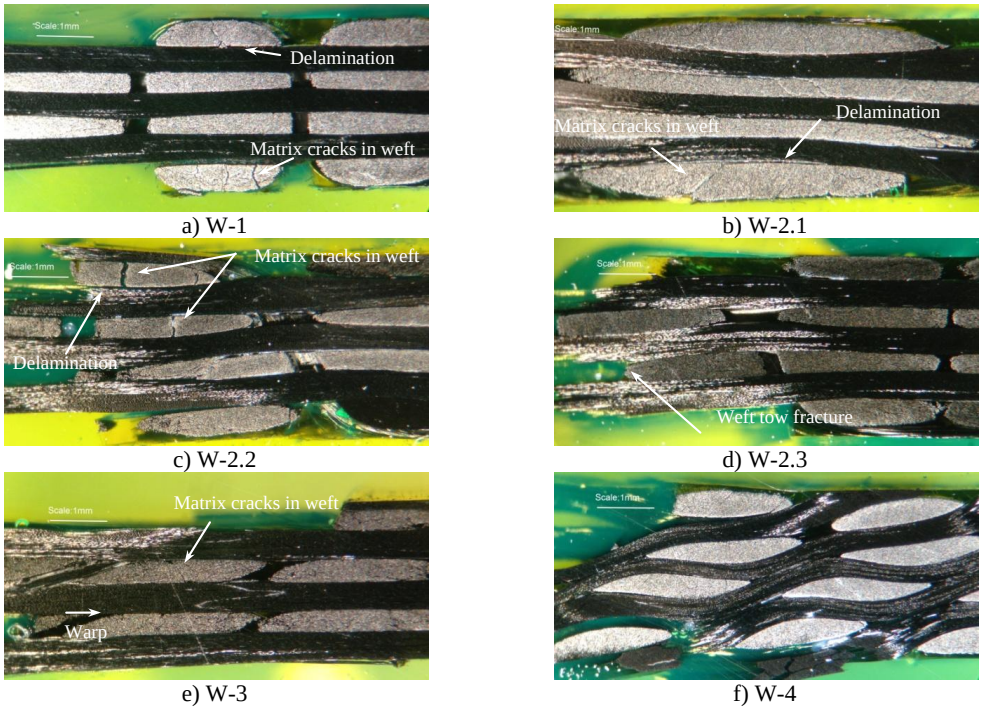

Figure 10: Failed sections of tensile samples (parallel to warp direction).

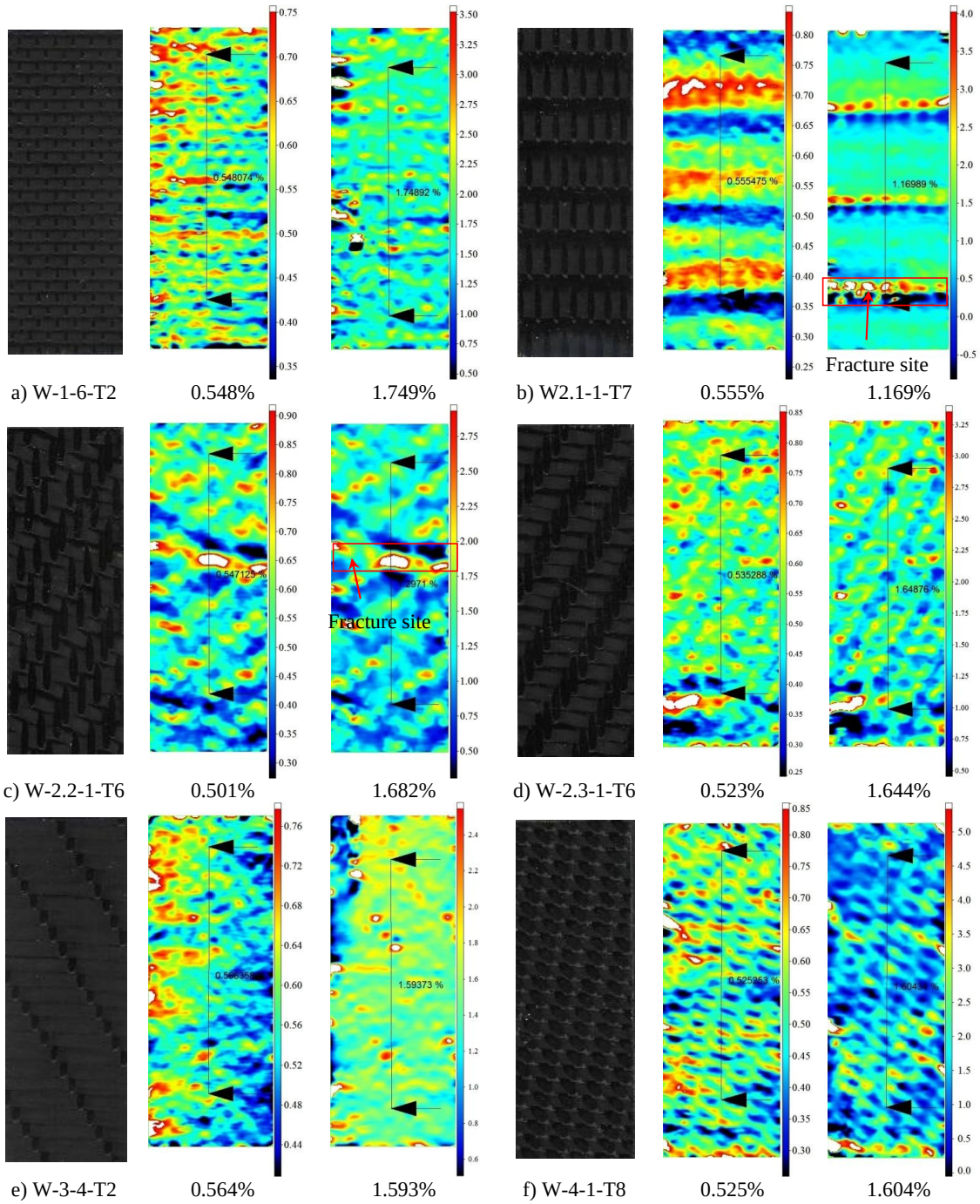

Figure 11: Axial strain (%) distributions at different strain level and the last frame before fracture.

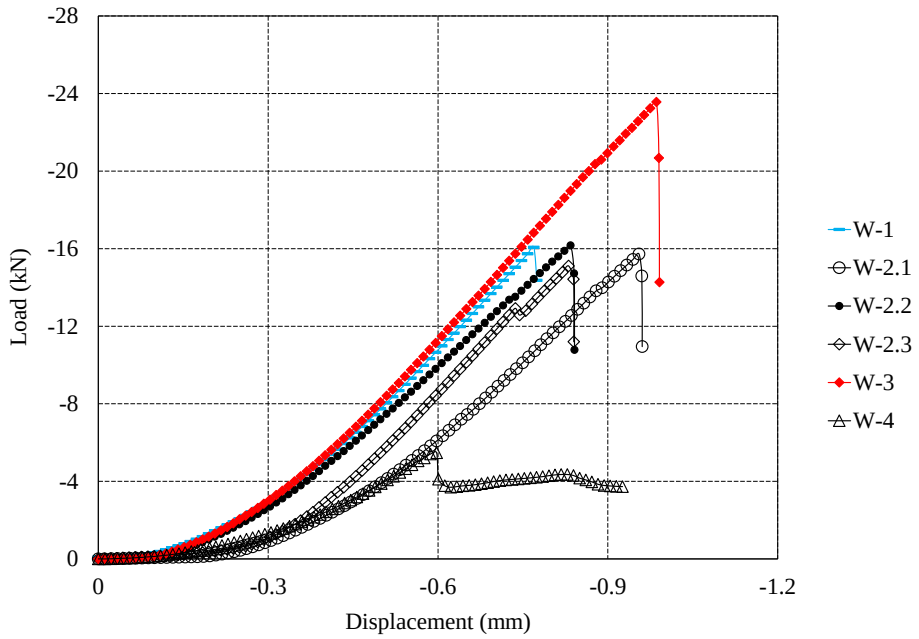

Figure 12: Typical load-displacement curves for all six types of woven composites under compression.

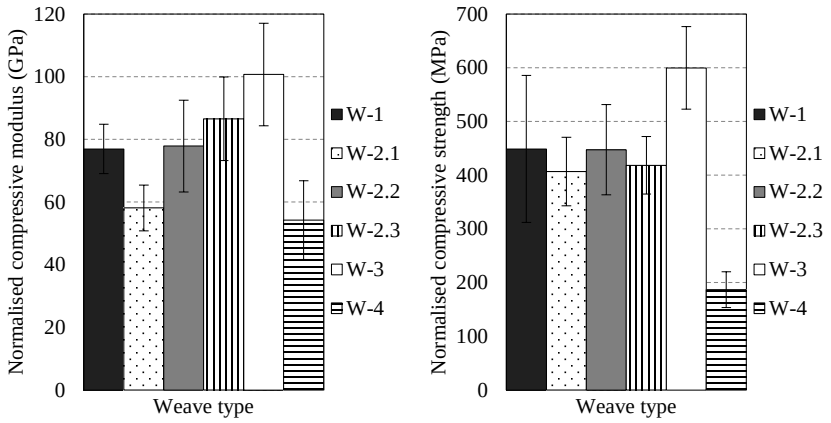

Figure 13: Normalised compressive properties.

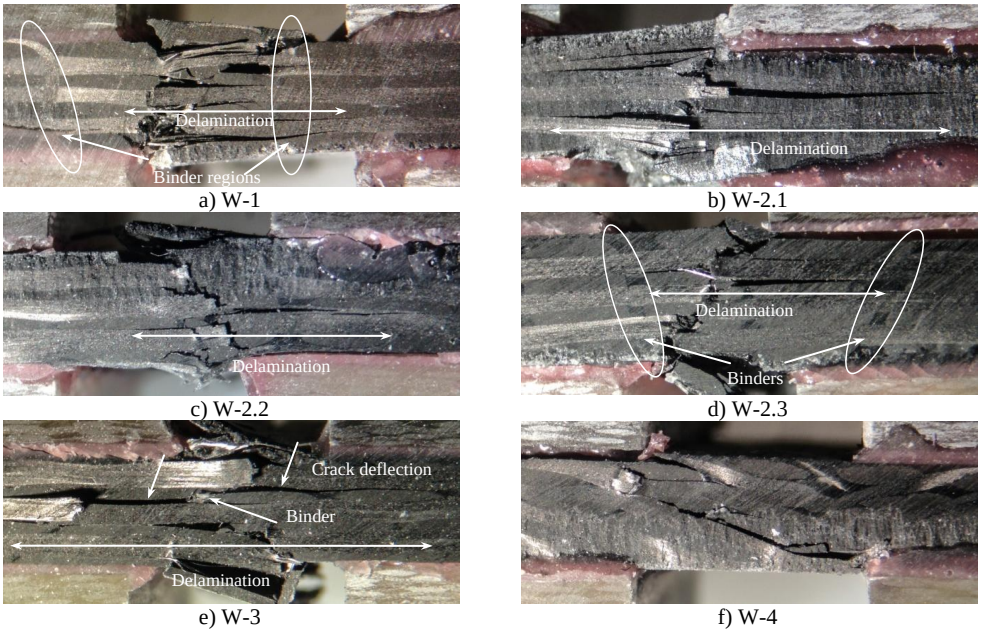

Figure 14: Failed sections of compression samples (parallel to warp direction).

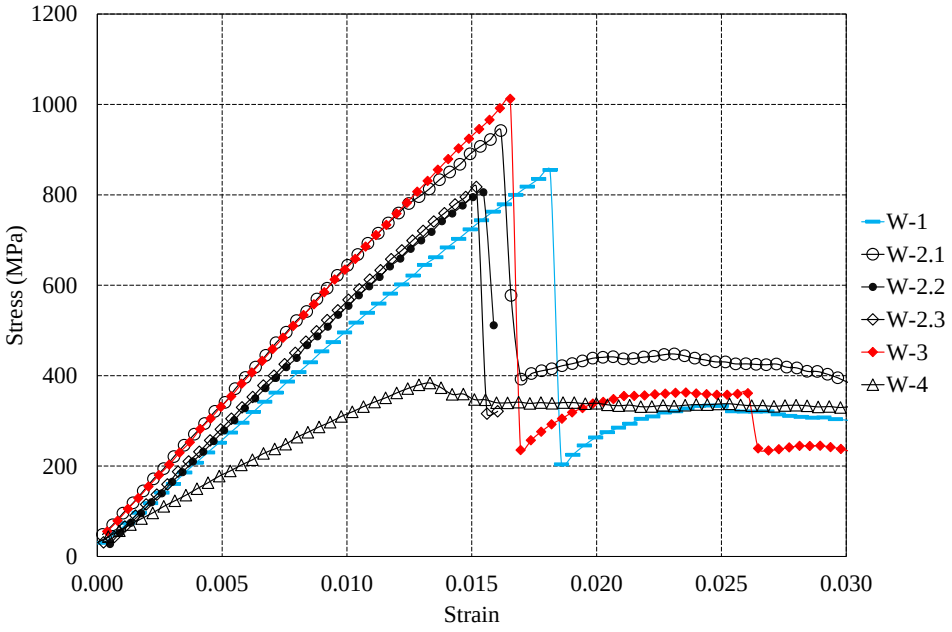

Figure 15: Typical stress-strain curves for all six types of woven composites under three-point bending.

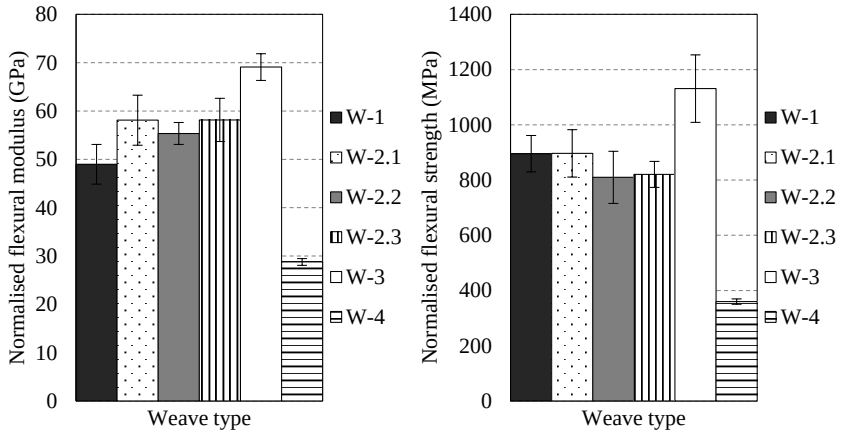

Figure 16: Normalised flexural properties.

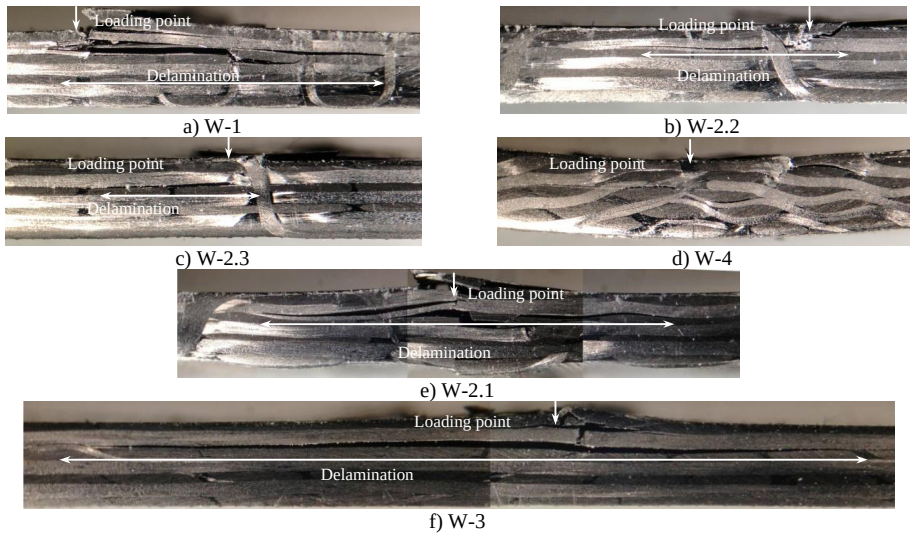

Figure 17: Failed sections of flexure samples (parallel to warp direction).

Table 1: Preform specification.

Weave type	ID	Binder tow		Warp tow		Weft tow	
		Type	Counts	Type	Counts	Type	Counts
Orthogonal 1×1	W-1	Toray T300	1k	IMS5131	24k	HTA40E13	2×6k
Orthogonal 3×3	W-2.1	Tairyfil T33	3k	IMS5131	24k	HTA40E13	2×6k
	W-2.2	Tairyfil T33	3k	IMS5131	24k	HTA40E13	2×6k
	W-2.3	Tairyfil T33	3k	IMS5131	24k	HTA40E13	2×6k
Angle interlock	W-3	Tairyfil T33	3k	IMS5131	24k	HTA40E13	2×6k
	W-4	IMS5131	24k	N/A	N/A	HTA40E13	2×6k

Table 2: Fibre volume fraction and thickness of the samples.

ID	V_f (%)	CV (%)	V_{warp} (%)	CV (%)	V_{weft} (%)	CV (%)	t (mm)	CV (%)
W-1	49.86	1.59	27.72	4.59	21.10	5.83	2.71	3.48
W-2.1	49.86	3.46	29.98	5.43	17.73	9.64	2.85	5.81
W-2.2	50.02	4.11	27.84	1.79	19.57	3.40	2.77	5.47
W-2.3	51.16	3.32	28.20	1.38	20.55	2.43	2.80	5.00
W-3	46.01	2.57	25.66	3.02	18.09	3.18	2.77	6.11
W-4	50.98	2.35	N/A	N/A	21.42	4.35	2.72	2.62

Table 3: Nominal sample geometries.

Test	Width (mm)	Length (mm)	Gauge (mm)	Shape
Tensile	25	250	150	Rectangular
Compressive modulus	15	80	10	Rectangular
Compressive strength	15	80	5	End-tabbed rectangular
Flexure	25	160	120	Rectangular

Table 4: Tensile properties.

Weave ID	Warp tow waviness (%)	Modulus (GPa)	CV (%)	Strength (MPa)	CV (%)
W-1	1.37	76.75	5.56	1358.54	3.22
W-2.1	2.83	69.44	29.53	1227.94	7.55
W-2.2	1.06	78.67	15.25	1103.17	6.61
W-2.3	1.40	73.46	10.48	1220.31	6.03
W-3	0.55	80.49	8.69	1276.24	5.96
W-4	N/A	48.54	13.44	409.90	4.91

Table 5: Compressive properties.

Weave ID	Modulus (GPa)	CV (%)	Strength (MPa)	CV (%)
W-1	76.18	10.22	444.31	30.46
W-2.1	62.21	12.57	435.59	15.67
W-2.2	77.41	18.81	444.80	18.84
W-2.3	87.19	15.40	421.41	12.82
W-3	92.29	16.27	549.59	12.76
W-4	57.25	23.18	197.41	17.84

Table 6: Flexural properties.

Weave ID	Modulus (GPa)	CV (%)	Strength (MPa)	CV (%)
W-1	48.49	8.42	886.48	7.36
W-2.1	62.22	8.87	960.12	9.54
W-2.2	55.04	4.14	805.26	11.65
W-2.3	58.57	7.70	826.52	5.74
W-3	63.32	4.04	1036.62	10.78
W-4	30.37	2.41	379.89	2.60